Directed hydroxyl radical probing reveals Upf1 binding to the 80S ribosomal E site rRNA at the L1 stalk

Anthony P. Schuller[1], Boris Zinshteyn[1], Syed Usman Enam[1] and Rachel Green[1,2,*]

[1]Department of Molecular Biology and Genetics, Johns Hopkins University School of Medicine, Baltimore, MD 21205, USA and [2]Howard Hughes Medical Institute, Johns Hopkins University School of Medicine, Baltimore, MD 21205, USA

ABSTRACT

Upf1 is an SF1-family RNA helicase that is essential for the nonsense-mediated decay (NMD) process in eukaryotes. While Upf1 has been shown to interact with 80S ribosomes, the molecular details of this interaction were unknown. Using purified recombinant proteins and high-throughput sequencing combined with Fe-BABE directed hydroxyl radical probing (HTS-BABE) we have characterized the interaction between Upf1 and the yeast 80S ribosome. We identify the 1C domain of Upf1, an alpha-helical insertion in the RecA helicase core, to be essential for ribosome binding, and determine that the L1 stalk of 25S rRNA is the binding site for Upf1 on the ribosome. Using the cleavage sites identified by hydroxyl radical probing and high-resolution structures of both yeast Upf1 and the human 80S ribosome, we provide a model of a Upf1:80S structure. Our model requires that the L1 stalk adopt an open configuration as adopted by an un-rotated, or classical-state, ribosome. Our results shed light on the interaction between Upf1 and the ribosome, and suggest that Upf1 may specifically engage a classical-state ribosome during translation.

INTRODUCTION

In eukaryotes there are several mRNA surveillance pathways that selectively degrade mRNAs and rescue ribosomes on mRNAs that are unlikely to produce biologically relevant products (1). One of these pathways, nonsense-mediated decay (NMD), selectively degrades mRNAs that contain what is broadly referred to as a premature termination codon (PTC). These mRNAs are created by multiple routes: genes may carry a mutation that results in a PTC (2), inefficient splicing may lead to export of a pre-mRNA with a PTC encoded in the intron (3,4), or the stop codons of upstream open reading frames (5,6) and non-coding RNAs

(7,8) can be sensed as PTCs. In these situations, the cell recognizes an mRNA with a PTC as a substrate for degradation, while those mRNAs with normal termination codons (TC) are maintained. This discrimination is still only partially understood, as NMD has been shown *in vivo* to regulate 1–10% of the transcriptome, demonstrating that NMD functions quite broadly in the regulation of gene expression (9–12).

The central molecular players of NMD in yeast, mammals and other eukaryotes are the three conserved 'upframeshift' proteins Upf1, Upf2, and Upf3 which were originally isolated in genetic screens for increased frameshifting output (13,14). Upf1 is the catalytic component of this complex, structurally organized into an N-terminal cysteine-histidine-rich (CH) domain that interacts with Upf2 and other proteins, and a RecA-like helicase core (SF1 family) that is responsible for RNA-dependent ATPase and helicase activities (15–18). In contrast, Upf2 and Upf3 are thought of primarily as interacting partners that regulate when and where Upf1 activity is implemented (9,16,19). In mammals NMD is more complex, where additional factors (such as the Smg5–7 proteins) coordinate their activities with the Upf proteins to elicit decay (20). Additionally, there is substantial evidence to suggest that much of NMD in these systems depends on interactions of the Upf proteins with the exon-junction complex that is deposited in the nucleus at splice junctions (21,22). While there is considerable molecular understanding of interactions between the Upf proteins and their binding partners in both yeast and mammals (9,20), we know little about the earliest events that trigger NMD on a particular RNA in either system. It has long been known that translation is required for NMD (23,24), and it stands to reason that events on the ribosome at the premature termination codons will be critical. It also has been shown that Upf1 migrates with polysomes (25), binds ribosomal protein eS26 in isolation (26), and has been found to interact with eukaryotic release factors (27), but the molecular details of interactions with intact ribosomes remain poorly characterized.

Using purified components and a <u>h</u>igh <u>t</u>hroughput <u>s</u>equencing-based Fe-BABE directed hydroxyl radical prob-

ing method (HTS-BABE) we have characterized the interaction between Upf1 and the 80S ribosome. We identify the L1 stalk of the 25S rRNA as the binding site for Upf1 on 80S ribosomes, and show that this interaction is dependent on the 1C domain of Upf1, a small alpha-helical insertion in the RecA helicase core. Our Fe-BABE probing data and structural modeling with high-resolution structures of the human 80S ribosome and Upf1 allow us to propose that the interaction between Upf1 and the L1 stalk requires an open configuration of the ribosome, such as that populated by ribosomes with tRNAs bound in a classical state. Taken together our results shed light on this interaction between Upf1 and the ribosome, and suggest that Upf1 may specifically bind a classical-state ribosome during translation.

MATERIALS AND METHODS

Full-length Upf1 expression and purification

Full-length Upf1 proteins purified from *Saccharomyces cerevisiae* were used in initial ribosome pelleting experiments (Figure 1) and ATPase assays (Supplementary Figure S1). The Upf1 gene from *S. cerevisiae* (NAM7) was cloned into pYES-DEST52 (Invitrogen) with TEV protease-cleavable N-terminal His_7 and C-terminal maltose binding protein (MBP) tags for affinity purification. All variants of Upf1 (point mutants and truncations) were prepared by sub-cloning from this parent plasmid using Topo Directional cloning (Invitrogen) or QuickChange mutagenesis (Stratagene). The pYES-DEST52 plasmid contains a *GAL1* inducible promoter for expression of Upf1 in *S. cerevisiae*. All full-length Upf1 proteins were expressed in *S. cerevisiae* JC287 (MATa, *ade2-1, his3, leu2, trp1, ura3, pep4::HIS3, prb1::HIS3, prc1::HIS3*) (provided by Dr. Jeff Coller) with 2% galactose. Cell pellets were harvested, flash frozen in A500 buffer (25 mM Tris, pH 7.5, 500 mM NaCl, 10% glycerol, 1 mM $MgCl_2$, 1 μM $ZnCl_2$ and 5 mM 2-mercaptoethanol), and lysed in a liquid nitrogen Freezer/Mill (SPEX Sample Prep, LLC). Cell lysates were purified over an amylose column (NEB) followed by a His-TrapFF column (GE Healthcare) to yield pure full-length Upf1 protein. Protein fractions were pooled, concentrated, exchanged into buffer A150 (same as A500 but with 150 mM NaCl and 1 mM DTT instead of 2-mercaptoethanol) and stored at –80°C. In our pelleting assays, the His and MBP tags were not cleaved from Upf1 as initial experiments showed they did not affect function (Supplementary Figure S1B).

Ribosomal subunit purification and pelleting assay

Ribosomal subunits from *S. cerevisiae* were purified as previously reported (45), or from *Escherichia coli* as previously reported (59). Ribosome pelleting assays were conducted by incubating ribosomal subunits with Upf1 proteins in reactions containing 100 nM 40S and 60S ribosomal subunits, 100 nM Upf1, 1 mM nucleotide, and 0.2 mg/ml polyU (Sigma) in 1X Buffer E (20 mM Tris, pH 7.5, 100 mM KOAc pH 7.5, 2.5 mM Mg(OAc)₂, 0.25 mM spermidine and 2 mM DTT). Reactions were pelleted over sucrose cushions containing 1.1 M sucrose in Buffer E using a Beckman MLA-130 rotor at 75 000 rpm for 1 hour at 4°C. Pelleted

ribosomes were resuspended in Buffer E and run on SDS-PAGE gels for Western blotting using an anti-MBP antibody (NEB) to detect Upf1.

Upf1 221–851 expression and purification

With the exception of Figure 1 and Supplementary Figure S1, all experiments used this *E. coli* purified Upf1 construct or variants of this construct as described. Residues 221–851 of the Upf1 gene were cloned into a plasmid containing a TEV protease-cleavable N-terminal His_6-MBP tag (pDESTHisMBP). Each construct was designed to include an N-terminal HA-tag in order to observe ribosome pelleting by Western blot analysis. This Upf1 construct was transformed into Rosetta 2 (DE3) pLysS competent cells (Novagen) and expressed overnight in terrific broth (RPI) in the presence of 500 μM IPTG at 16°C. Cells were lysed by French press (Thermo) in A500 buffer and purified using amylose resin (NEB). Fractions containing Upf1 protein were then pooled, and incubated with His-tagged TEV protease overnight to remove the His_6-MBP tag on Upf1. After cleavage, proteins were further purified over Ni-NTA resin (Qiagen) to remove both the free His_6-MBP and His_6-tagged TEV protease, and a Superose 6 10/300 GL column to ensure the protein was not aggregated. Purified Upf1 was stored in A150 buffer at -80°C for subsequent assays.

For Fe-BABE probing experiments, the Upf1 Δ4cys (C709A, C777A, C833A, C845A) parent construct was created by QuickChange mutagenesis of the pDESTHisMBP expression plasmid for Upf1 221–851. Using this Upf1 Δ4cys clone, additional cysteine mutations (one per construct) were made by QuickChange mutagenesis to engineer sites for Fe-BABE modification (Figure 3A). All expression plasmids were verified by Sanger sequencing to confirm the sequence.

Fe-BABE labeling and rRNA cleavage

eIF5A site-specific cysteine variants were labeled with Fe-BABE by first dialyzing 40 μl of 40 μM protein into eIF5A modification buffer (30 mM Hepes, pH 7.5, and 500 mM KCl) for 5.5 h at 4°C. After dialysis, each eIF5A variant was labeled by incubation with 2 mM Fe-BABE (Dojindo Molecular Technologies) at 30°C for 30 min. After labeling, the proteins were concentrated and buffer exchanged into Fe-eIF5A storage buffer (20 mM Hepes, pH 7.5, 100 mM KCl, and 3 mM $MgCl_2$), and stored at –80°C.

Upf1 site-specific cysteine variants were labeled using a similar protocol with a few modifications for Upf1 protein stability. 40 μl of 40 μM Upf1 protein was dialyzed into Upf1 modification buffer (30 mM Hepes, pH 7.5, 10% glycerol, and 500 mM KCl) for 5.5 h at 4°C. After dialysis, each Upf1 variant was labeled by incubation with 2 mM Fe-BABE (Dojindo Molecular Technologies) at 30°C for 30 minutes, or in one circumstance at 4°C overnight (Figure 4B labeled as 'o/n'). After labeling, the proteins were concentrated and buffer exchanged into Fe-Upf1 storage buffer (20 mM Hepes, pH 7.5, 150 mM KCl, 10% glycerol and 3 mM $MgCl_2$), and stored at –80°C.

rRNA cleavage was performed as a 20 μl reaction containing 500 nM 80S ribosomal subunits (purified as described above), 500 nM Fe-BABE-labeled protein (eIF5A
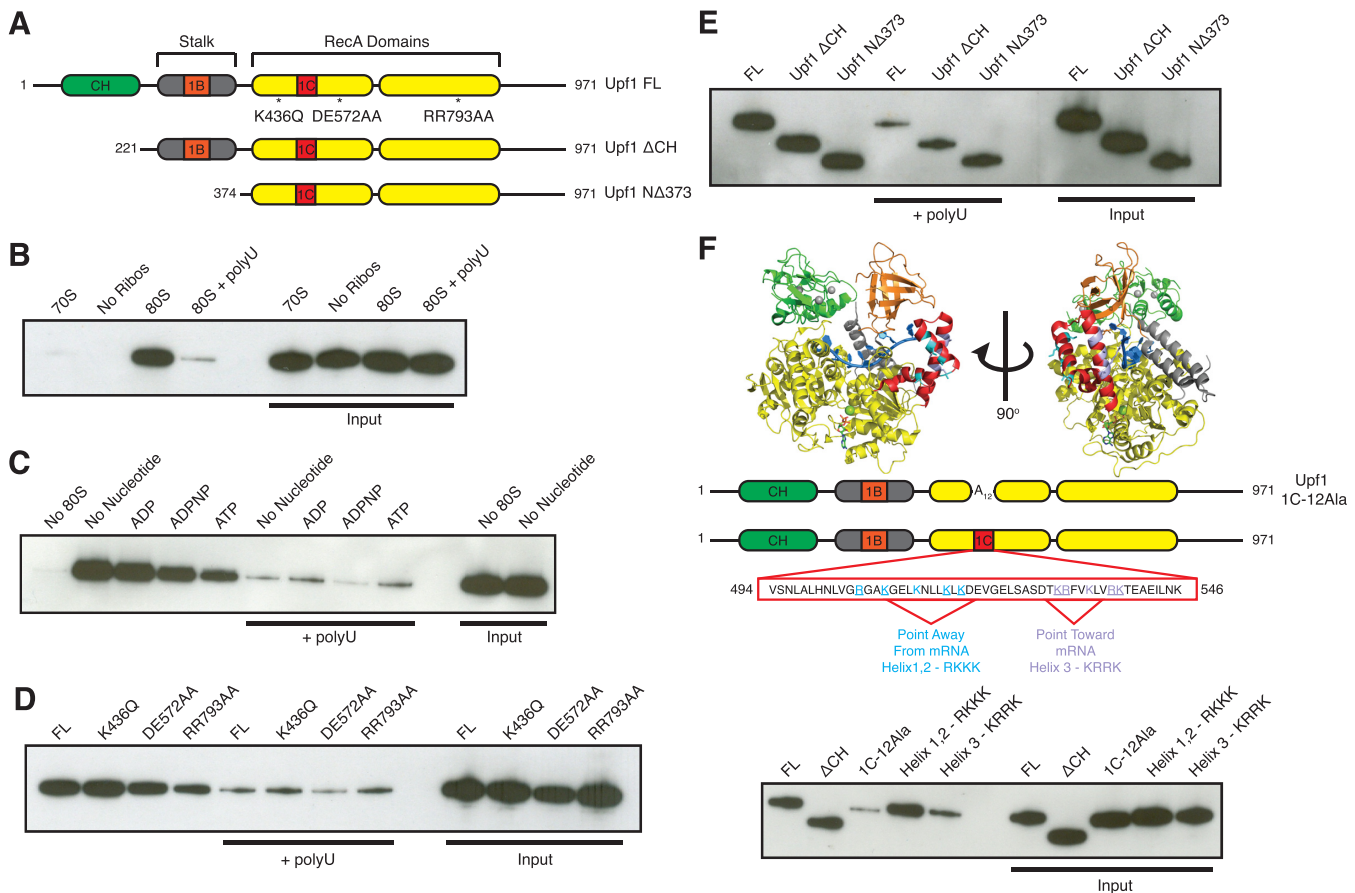
Figure 1. Upf1 binds 80S ribosomes via 1C domain. (**A**) Schematic of Upf1 domain structure with point mutants and domain truncation constructs used in ribosome pelleting assays. (**B**) Upf1-ribosome pelleting assay comparing association with *S. cerevisiae* 80S ribosomal subunits and *E. coli* 70S ribosomal subunits. (**C**) Upf1-ribosome pelleting assay with different ATP analogs added, or no nucleotide. (**D**) Upf1-ribosome pelleting assay using various Upf1 point mutants for ATP binding (K436Q), ATP hydrolysis (DE572AA), and weakened mRNA binding (RR793AA). (**E**) Upf1-ribosome pelleting assay using Upf1 N-terminal domain truncation constructs as detailed in panel (A). (**F**) Upf1-ribosome pelleting assay using construct where 1C domain is replaced by a stretch of 12 alanines (1C-12Ala), or where specific positively charged surface sites are substituted with alanine. Structure of Upf1 with 1C domain shown in red and mRNA in blue (PDB 2XZL). Positive residues (Lys and Arg) on each side of the 1C domain are colored in cyan (Helix 1, 2) and light purple (Helix 3).

or Upf1) in cleavage buffer (20 mM Hepes, pH 7.5, 100 mM KCl and 3 mM MgCl$_2$). Reactions were incubated on ice for 15 minutes to allow factor binding. Then we added 1 μl of 100 mM ascorbic Acid, and 1 μl fresh 0.5% hydrogen peroxide simultaneously to initiate radical generation. Pipetting each 1 μl reactant on the wall of a microcentrifuge tube, and then quickly spinning the contents allowed for simultaneous mixing. The reaction continued on ice for 15 minutes and was then quenched by addition of 1 μl of 100 mM thiourea and 300 μl of rRNA extraction buffer (0.3 M NaOAc). The rRNA was then extracted by acid phenol, phenol:chloroform (5:1), and subsequently ethanol precipitated and resuspended in nuclease-free H$_2$O.

HTS-BABE method and analysis

The HTS-BABE method contains several steps: (i) reverse transcription of the cleaved rRNA, (ii) cleanup by RNA-Clean XP beads (Agencourt), (iii) 3′ end ligation by Circligase (Epicentre), (iv) Cleanup by Ampure XP beads (Agencourt), (v) PCR and gel extraction of products and (vi) Illu-

mina sequencing. As previously mentioned, our method is based on one recently published (37) with several modifications we have described here.

In step i, the cleaved rRNA is reverse transcribed (RT) using a random nonamer (SN$_8$)-oligo (oAS544). 1 μg of cleaved rRNA was incubated with 20 μM oAS544 in 1X RT-Mg buffer (50 mM Tris–Cl, pH 8.6, 60 mM NaCl, 10 mM DTT) at 65°C for 5 min and then moved to ice to allow annealing of the oligo on the rRNA. Then 5 μl of this annealed-mixture was added to a mixture containing 2.5 μl 5X dNTP mix (1.7 mM of each dNTP), 2.5 μl 1X RT+Mg buffer (50 mM Tris-Cl, pH 8.6, 60 mM NaCl, 10 mM DTT, 6 mM MgCl$_2$) and 2.5 μl RVT mix (0.25 μl 10X RT-Mg buffer, 0.25 μl SSIII reverse transcriptase (Thermo), and 2 μl H$_2$O) to yield a final volume of 12.5 μl. This reaction was then reverse transcribed by incubating as follows: 25°C – 10 min, 50°C – 70 min, 60°C – 10 min, 4°C – indefinite. After the reaction completed, we incubated at 70°C for 15 min to denature the reverse transcriptase and then added 25 μl of 1X RT + Mg buffer to make a final volume of 37.5 μl. The reaction was then subjected to RNaseH digestion by adding

1 μl of RNAseH (NEB) and incubating at 37°C for 20 min to digest the rRNA.

In step ii, the resulting reverse transcription product is purified by RNAClean XP beads. We added 67.5 μl of beads to each reaction, and incubated at room temperature for 30 min, mixing the components every 10 min. Then the supernatant was removed after placing the reactions on a magnetic stand for 5 min. We subsequently washed with 200 μl of 70% EtOH two times, and eluted with 40 μl of 5 mM sodium citrate, pH 6.0. To elute, the beads were mixed with buffer and incubated at 37°C for 10 min, then placed on the magnetic stand and the eluant removed.

In step iii, the cDNA product is ligated with a 3′ linker for future sequencing steps. In this reaction, we mixed 3 μl of each cDNA product with a 7 μl ligation mix containing 1 μl 10X Circligase buffer, 0.5 μl 1 mM ATP, 0.5 μl 50 mM MnCl$_2$, 2 μl 50% PEG 6000, 2 μl 5 M betaine, 0.5 μl of 100 μM oAS545 linker and 0.5 μl Circligase enzyme. The resulting 10 μl reaction was incubated as follows: 60°C – 120 min, 68°C – 60 min, 80°C – 10 min, 4°C – indefinite. Then we added 10 μl H$_2$O for a final volume of 20 μl to proceed.

In step iv, this ligated cDNA product is purified using Ampure XP beads. The procedure is similar to step 2 with the following exceptions: (i) We used 36 μl of beads to clean the 20 μl sample and (ii) We eluted using 16 μl of H$_2$O.

In step v, the purified cDNA is amplified using PCR primers containing adaptor sequences for Illumina sequencing and barcodes for sample multiplexing. Our PCR reactions contained 6 μl of ligated cDNA product, 3.6 μl of 10 μM Index oligo (oASBar01–30), 3.6 μl of 10 μM forward oligo oBZ287, 12 μl 5X Phusion HF Buffer, 4.8 μl 2.5 mM dNTPs, 28.8 μl H$_2$O, and 1.2 μl Phusion DNA polymerase. Our amplification protocol was as follows: 98°C – 3 min, (98°C – 80 s, 64°C – 15 s, 72°C – 30 s) repeated 4 times, (98°C – 80 s, 72°C – 45 s) repeated 10 times, 72°C – 5 min, 4°C – indefinite. The PCR reactions were then run on an 8% TBE native gel at 200 V for 28 min and stained with SYBR gold. The resulting products >150 bp were cut from the gel and extracted overnight in 0.3 M NaOAc with 1 mM ETDA at room temperature. We intentionally cut >150 bp to avoid sequencing the amplified product that results from ligation of the unextended RT oligo directly to the 3′ linker (and therefore contains no insert cDNA). The following day, the extracted DNA was precipitated with isopropanol and quantified using an Agilent 2100 Bioanalyzer before sequencing.

The amplified products were subjected to 50 bp single-end sequencing on an Illumina HiSeq 2500 and subjected to our analysis pipeline. The reads are first trimmed of the 3′ adaptor using the skewer package (60). The N$_7$ randomized nucleotides from our ligated adaptor were trimmed from read 5′ ends using fastx_trimmer (http://hannonlab.cshl.edu/fastx_toolkit/index.html by Hannon Lab). The read 5′ end now corresponds to the 5′ nucleotide of the 3′ product resulting from radical cleavage. Next, the reads were mapped to the yeast ribosomal rRNA (including 25S, 18S, 5.8S and 5S) using STAR (61) to provide a normalized (reads per million, rpm) read 5′ end count at each rRNA nucleotide.

To analyze our data, we compared the rpm at each rRNA nucleotide for each site-specific cysteine variant with the eIF5A Δcys or Upf1 Δ4cys controls. We simply divided the rpm at each nucleotide position across the ribosome to generate a fold-change of reads in the labeled variant compared to the control, and thereby to identify enhanced cleavage sites caused by the Fe-BABE label at a particular position.

Primer extension for rRNA cleavage analysis

To identify rRNA cleavage sites by primer extension analysis, first the cleaved rRNA must be reverse-transcribed with a radioactive site-specific oligo complementary to the rRNA sequence. Approximately 1 μg of cleaved rRNA is first mixed in a 5 μl reaction with a 32-P end-labeled oligonucleotide (200 nM) in 1X RT-Mg buffer and annealed by incubating at 60°C for 5 minutes and then moved to ice. 2 μl of this annealed-mixture was then added to a mixture containing 1 μl 5X dNTP mix (1.7 mM of each dNTP), 1 μl 1X RT + Mg buffer, and 1 μl RVT mix (0.25 μl 10X RT-Mg buffer, 0.25 μl AMV (Roche) and 2 μl H$_2$O) to yield a final volume of 5 μl. This reaction was then incubated at 42°C for 60 min for reverse transcription to occur. For sequencing ladders, the reactions contained 2 μl of the annealed-mixture, 1.3 μl 5X dNTP mix, 0.7 μl 5X ddNTP (0.2 mM of one ddNTP) and 1 μl RVT mix. The resulting cDNA products were mixed with 2X formamide loading dye and run on 10% TBE-Urea gels at 60W for 2–4hrs depending on the region to be analyzed.

ATPase Assays

Purified full-length Upf1 constructs (200 nM) were mixed with 0.02 mg/ml polyU (for Upf1 and Upf1 ΔCH) or 0.2 mg/ml polyU (for Upf1 1C-12Ala). Reactions were incubated at 26°C and time points quenched with 30% formic acid. Samples were spotted on PEI-Cellulose F TLC plates (EMD Millipore) and analyzed in 0.5 M KH$_2$PO$_4$ pH 3.5. TLC plates were developed using a Typhoon FLA 9500 Phosphorimaging system and quantified using ImageQuant TL (GE Healthcare Life Sciences).

***In vitro* reconstituted translation assays**

The elongation and termination assays were performed as previously described (38) using MFFFKX-UAA initiation complexes or MFX-UAA pre-termination complexes with the addition of 10–20 μM Upf1 ΔCH.

The recycling assay was performed using MFKX-UAA pre-termination complexes in reaction with 1X Buffer E, 4 μM AGQ-eRF1, 2 μM Rli1 and 10 μM Upf1 ΔCH. 50 μM peptidyl-tRNA hydrolase (PTH) was added to the reactions to quantify dissociated complexes (PTH cannot access the peptidyl-tRNA unless released from the ribosome) (46). Time points in both assays were quenched using 10% formic acid and run on electrophoretic TLC (Millipore).

All TLC plates were developed using a Typhoon FLA 9500 Phosphorimager system and quantified using ImageQuantTL (GE Healthcare Life Sciences). Time courses were fit to single exponential kinetics using Kaleidagraph (Synergy Software).

RESULTS

Upf1 directly interacts with 80S ribosome via 1C domain

Several previous studies have shown that Upf1 sediments with 80S ribosomes in polysome gradients (25) from cell lysate or binds ribosomal proteins in isolation (26). In an effort to better understand the molecular details of the interaction between Upf1 and 80S, we used *in vitro* purified proteins (including full-length Upf1 and many variants) (Figure 1A and Supplementary Figure S1A) and ribosomal subunits to perform ribosome-pelleting assays (Figure 1B–F and Supplementary Figure S1B). In these experiments, ribosomal subunits and Upf1 were spun through a sucrose cushion and the pellet analyzed by Western blot to determine the extent of ribosome-bound Upf1. In an initial reaction, full-length Upf1 efficiently pelleted with 80S yeast ribosomes (a mixture of both 40S and 60S subunits) but not bacterial 70S ribosomes (Figure 1B). These observations argue that the interaction between Upf1 and the eukaryotic ribosome is not simply due to the general RNA-binding activity of Upf1 since 70S ribosomes are thought to be equivalently rich in RNA. We also note that this ribosome binding activity was readily competed by the addition of polyU in the binding reaction (Figure 1B, lane 4), consistent with the fact that Upf1 is known to generally bind RNA and that its ATPase activity is stimulated by RNA (17).

Because the ATPase function of Upf1 is known to be critical for NMD in cells, we next evaluated the nucleotide dependence of the Upf1:80S interaction. Although Upf1 interacts with the ribosome under all nucleotide conditions (ATP, ADP, ADPNP, or no nucleotide), binding was most effective in the presence of ADP or no nucleotide relative to ADPNP or ATP (Figure 1C). These data correlate nicely with reported binding constants for the Upf1:polyU interaction under similar conditions (15), and further suggest that Upf1 might interact with both rRNA and mRNA through similar surfaces. We next asked whether known mutations in Upf1 that perturb ATP binding (K436Q), ATP hydrolysis (DE572AA), or RNA binding (RR793AA) impact the interaction with the ribosome. We found that Upf1 ATPase mutants DE572AA and K436Q efficiently pellet with the ribosome, while the RNA binding mutant (RR793AA) pelleted with reduced efficiency (Figure 1D). Each of these variant proteins was as equivalently competed away from the ribosome by an excess of polyU RNA as the wild-type Upf1.

Previous reports suggested a role for the N-terminal CH domain of Upf1 in interaction with the ribosome (26). To test this directly, we purified a variant of Upf1 lacking this domain as well as a more severe truncation containing only the helicase core of Upf1 (Figure 1A; Upf1 ΔCH and Upf1 NΔ373 respectively). Ribosome pelleting assays with these constructs showed that the CH domain was not critical for ribosome binding *in vitro* (Figure 1E). Interestingly, even the Upf1 helicase core (Upf1 NΔ373) was efficiently pelleted though binding by this variant protein was less efficiently competed by polyU (likely because much of the mRNA binding surface area contained in the CH and 1B domains has been removed).

We next focused on the 1C domain of Upf1, a small, conserved insertion in the first RecA domain of Upf1 that is comprised of a three alpha-helix bundle that positions two positively charged patches on the surface of Upf1. One surface points away from the previously defined mRNA binding channel (Helix 1,2) (Figure 1F, cyan residues) and another points toward the mRNA binding channel (Helix 3) (Figure 1F, light purple residues). We first generated a Upf1 variant where the 1C domain (residues V494-K546) was substituted with a stretch of twelve alanine residues (Upf1 1C-12Ala) and found that Upf1 binding to the ribosome was very nearly abolished (Figure 1F, lane 3). More selective alanine substitution of several positively charged patches on either of two sides of the helical bundle revealed Helix 3 as the more critical surface for ribosome binding (Figure 1F, lane 5). This same surface has previously been shown in X-ray structures to be involved in mRNA binding (15). In fact, substitution of the 1C domain with 12 alanines greatly weakens the mRNA binding ability of Upf1 as evidenced by our data (Supplementary Figure S1C) and others (28). Taken together, our results indicate that Upf1 binds the ribosome (and likely the ribosomal RNA) through the positively charged 1C domain and are consistent with a dual-binding mode for this domain that could allow Upf1 to partition between mRNA and the ribosome during NMD.

Development of HTS-BABE method using eIF5A

In order to more precisely define the site of interaction between Upf1 and 80S ribosomes, we pursued a hydroxyl radical probing approach using site-specific Fe-BABE labeling. Radical probing/footprinting has been used for decades to identify protein binding sites on the ribosome (29). This approach works by using Fenton chemistry to create hydroxyl radicals (in the presence of Fe(II), hydrogen peroxide, and ascorbic acid) that directly cleave nucleic acid backbone (30). To add an additional layer of control to this reaction, Fe-BABE (Fe(II)-bromoacetamidobenzyl-EDTA) molecules can be site-specifically conjugated at cysteine residues on a protein of interest to spatially localize hydroxyl radical generation (31). In this way, hydroxyl radicals are created at the Fe-BABE modification site and can diffuse as far as ∼40 Å to cleave rRNA (32). This directed-probing has been used successfully to map protein binding sites on the ribosome (33–35) as well as conformational rearrangements that occur during translation (36). The cleaved rRNA bases are detected by reverse transcriptase stops in a primer extension reaction when comparing a sample that has been labeled with Fe-BABE at a particular location to one lacking this modification. Although this method has proven powerful over the years, one limitation of the technique is that it requires many primer extension reactions and gels to identify cleavage sites across the entire ribosomal rRNA, which is costly and extremely time consuming.

To improve this method, we adapted Fe-BABE-mediated rRNA cleavage detection to high-throughput sequencing technology (HTS-BABE, Figure 2A) as recently described for a solution-based experiment aimed at defining the accessible surface area of the *E. coli* 16S rRNA (37). Our method uses directed hydroxyl radicals created at a site-specific Fe-
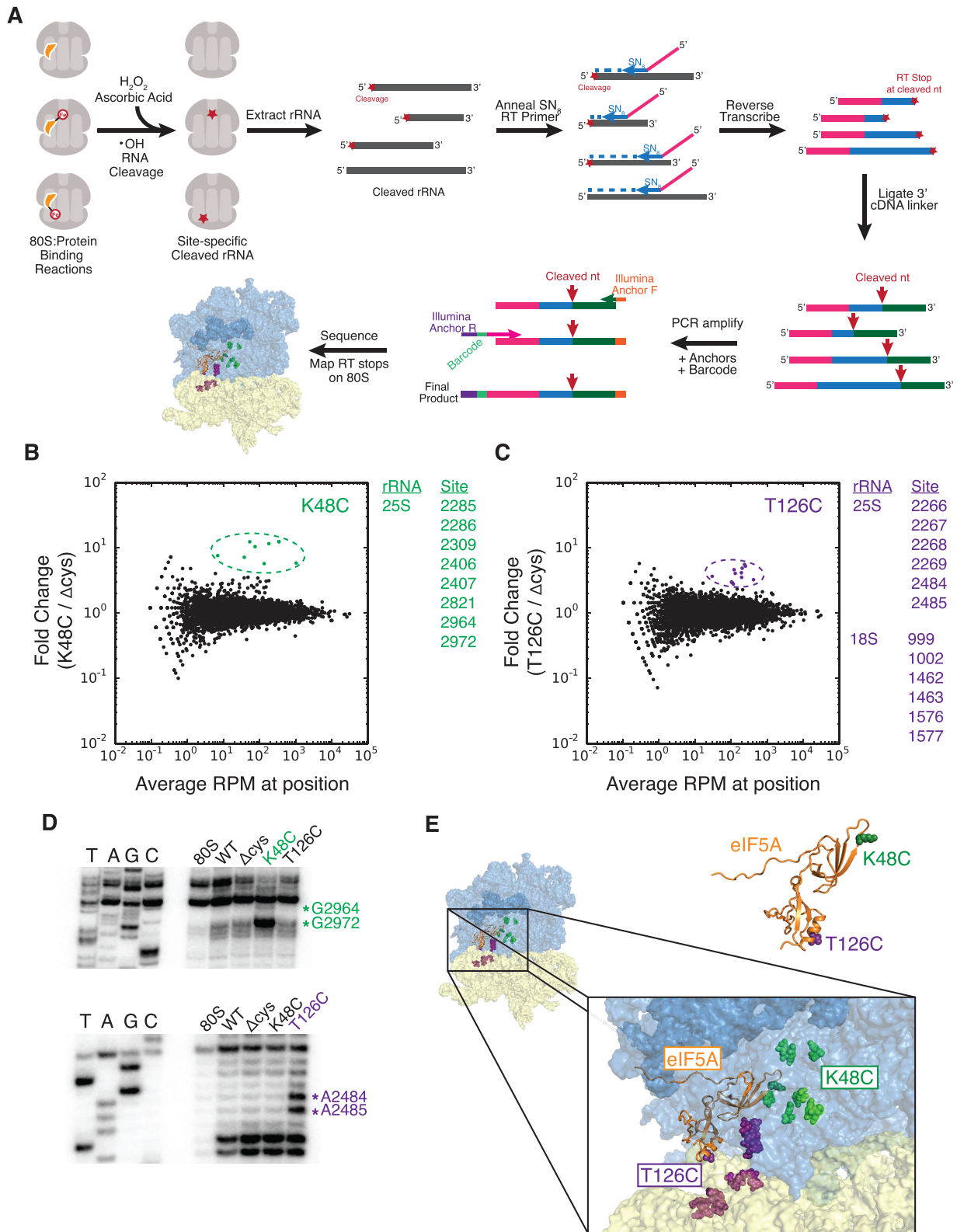
Figure 2. HTS-BABE method development and determination of eIF5A binding site on yeast 80S ribosomes (test case). (**A**) Schematic of HTS-BABE workflow. Briefly, cleaved rRNA is isolated and reverse-transcribed using a random SN_8 oligomer. cDNAs are ligated to a 3′ linker and amplified for Illumina sequencing to identify cleavage sites. (**B**) MA plot for eIF5A site-specific cysteine variant at position K48C and its corresponding rRNA cleavage sites identified using HTS-BABE. (**C**) Same as (**B**) for position T126. (**D**) Primer extension gels to confirm target sites identified by HTS-BABE method for both eIF5A K48C and T126C. (**E**) Structural model of eIF5A bound to 80S ribosome (PDB 5GAK) with Fe-BABE label locations (K48C – green, T126C – purple) and their corresponding cleavage sites as identified by HTS-BABE.

BABE moiety, rather than those created in solution, to allow for high resolution mapping of protein binding sites on the ribosome. We chose to test our method using eIF5A, a small protein known to bind the ribosomal E where it stimulates global translation elongation and termination (38). eIF5A was an ideal candidate to test our method because Fe-BABE probing has previously been used to map its specific ribosome binding site (39), and a recently determined high-resolution cryoEM structure verified this initial positioning (40).

We expressed and isolated from *S. cerevisiae* two previously characterized site-specific cysteine variants of eIF5A (K48C and T126C) and a 'scrubbed' version of eIF5A where all cysteines were removed (native C23A and C39T mutated; called eIF5A Δcys) (Supplementary Figure S2A). These proteins were modified with Fe-BABE and subjected to our HTS-BABE approach (Figure 2A). The method begins by incubating ribosomal subunits and Fe-BABE labeled eIF5A proteins in the presence of ascorbic acid and hydrogen peroxide to initiate Fenton chemistry and hydroxyl radical cleavage. The reactions are then quenched by addition of thiourea, and the ribosomal RNA from each reaction with Fe-BABE labeled protein or the eIF5A Δcys control is isolated. Subsequently, this cleaved rRNA is reverse transcribed using a random nonamer (SN$_8$)-containing oligonucleotide and superscript III reverse transcriptase to reveal cleaved bases as reverse transcriptase stops. These cDNA fragments are then subjected to a 3′ linker ligation and subsequent amplification using barcoded primers for Illumina sequencing (see Methods and Materials for details).

To identify the rRNA cleavage sites, we mapped our sequencing reads to each of the *S. cerevisiae* ribosomal RNAs and compared the number of RT stops at each position for each Fe-BABE variant with the eIF5A Δcys control. To identify robust cleavage sites, we focused on nucleotide positions with a fold change >2.5 (ratio of cys-variant/Δcys) that were also outliers from the rest of the distribution. For eIF5A K48C, we found strongly enhanced rRNA cleavage at eight positions in the 25S rRNA compared to eIF5A Δcys (Figure 2B and Supplementary Figure S2B). For eIF5A T126C, we found enhanced cleavage at 6 nucleotides of the 25S rRNA and six nucleotides in the 18S rRNA (Figure 2C and Supplementary Figure S2C). Many of these sites overlap with those identified in previous Fe-BABE probing experiments evaluated with primer extension gels (39); we also confirmed several of these cleavage sites using primer extension gel analysis (Figure 2D). Importantly, these locations mapped onto the 80S ribosome structure nicely clustered within 30 Å of the modified cysteine in the context of the previously solved cryoEM structure (Figure 2E and Supplementary Figure S2D and E) (40). These experiments performed with eIF5A establish that this method can readily identify Fe-BABE hydroxyl radical cleavage locations without the need for primer extension gels. Moreover, with proper multiplexing of samples, it is possible to obtain data for many Fe-BABE variants in a single sequencing lane.

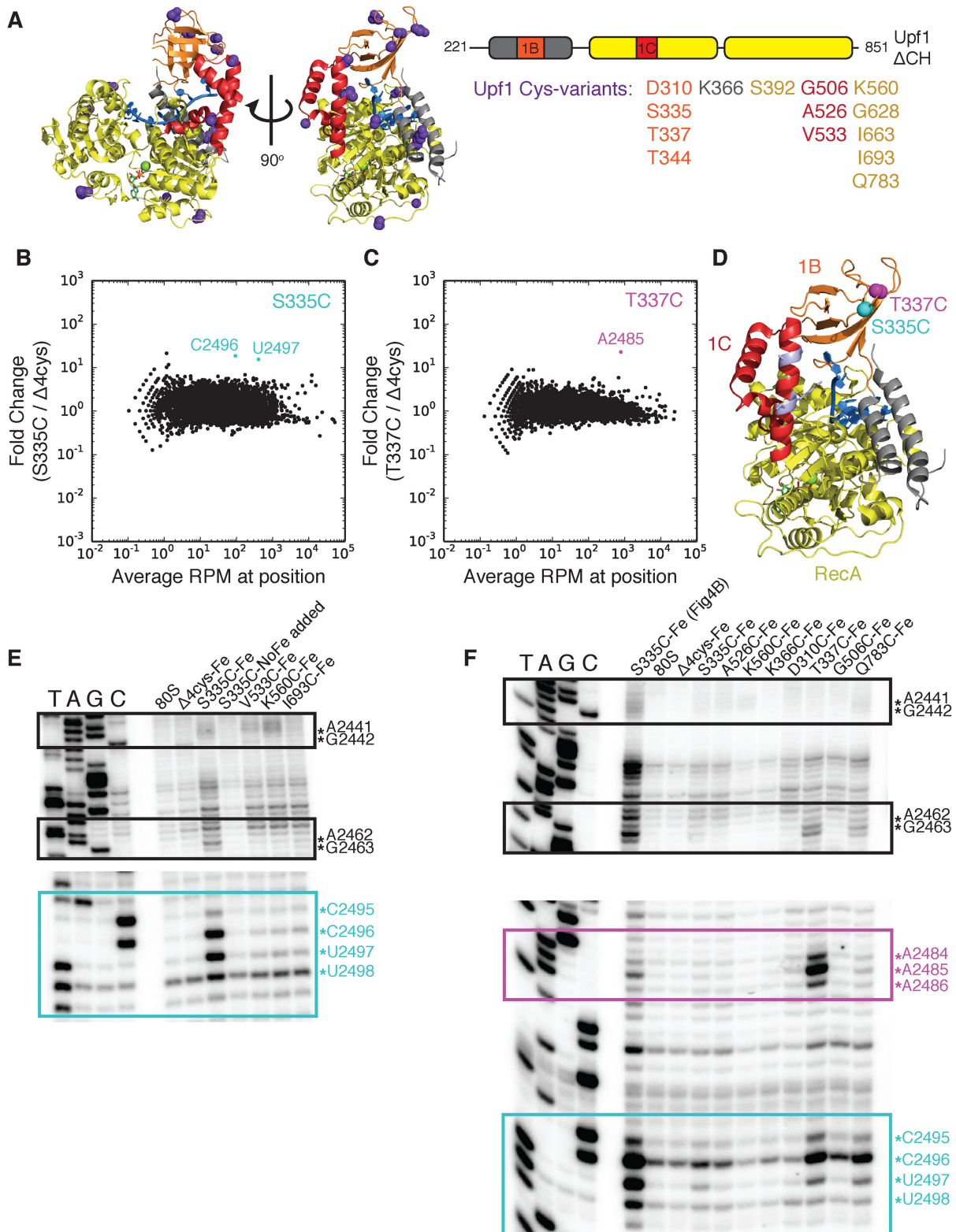### HTS-BABE reveals Upf1 binding to 25S ribosomal RNA

We next performed a similar HTS-BABE experiment with Upf1 (and 14 distinct site-specific cysteine variants) and the 80S ribosome (Figure 3A and Supplementary Figure S3A). As the Upf1 CH domain is cysteine-rich but dispensable for ribosome binding (Figure 1E), we chose a Upf1 ΔCH parent construct for this experiment (residues 221–851) (Supplementary Figure S3B-C). While this truncated Upf1 construct contained nine natural cysteines, the crystallographic structure suggested that 5 were not adequately surface-exposed for Fe-BABE modification and were thus left as is. We determined that the remaining four cysteines could be removed to create soluble, non-aggregated Upf1 (C709A, C777A, C833A, C845A; called Upf1 Δ4cys). This parent construct was then mutated to create site-specific cysteine variants that span the entire surface of Upf1, with several localized on or near the ribosome-binding 1C domain that we identified above (Figure 1F). These Upf1 variants were expressed and purified from *E. coli* (see Materials and methods), labeled with Fe-BABE, and subjected to the same HTS-BABE method developed for eIF5A.

Our HTS-BABE analysis for these site-specific Upf1 Fe-BABE variants revealed two variants with sites of strongly enhanced rRNA cleavage compared to the Upf1 Δ4cys control. Upf1 S335C showed enhanced cleavage (outliers from the MA plot) at 25S C2496 and U2497 (19- and 15-fold respectively) of Helix 76 (Figure 3B and Supplementary Figure S3D) and T337C showed enhanced cleavage at 25S A2485 (23-fold) near the L1 binding loop (Figure 3C and Supplementary Figure S3E). Both variants are positioned on the 1B domain of Upf1 that is spatially located adjacent to the ribosome-binding 1C domain (Figure 3D) (i.e. the key residues identified as critical to ribosome binding in Figure 1F). Traditional primer extension analysis for Upf1 S335C (Figure 3E) and T337C (Figure 3F) confirmed these strong rRNA cleavage locations, and also identified other weaker cleavage sites near this region of the 25S rRNA for these variants and several others.

Upf1 1C domain is required for interactions with L1 stalk

The cleavage sites identified by Upf1 Fe-BABE probing map to the 25S L1 stalk located near the ribosomal E site (Figure 4A). This region of the ribosome has been shown to undergo large-scale movements throughout translation elongation in *E. coli* (41). In classical-state ribosomes, where the E site is empty, the L1 stalk adopts an 'open' conformation, oriented away from the ribosome core. After peptidyl-transfer, the deacylated tRNA (having just transferred the peptidyl group to the A-site tRNA) adopts a hybrid P/E state, and the L1 stalk moves inward to make interactions with the tRNA elbow in a 'closed' state. Next the L1 stalk moves through two 'intermediate-closed' positions as the tRNA moves through a pe/E chimeric hybrid state, and finally into a classical E/E state. The stalk maintains interactions with the tRNA elbow in these intermediate states, so release of the E-site tRNA likely occurs after the stalk fully opens again.

As this region of the ribosome is RNA-rich and flexible, we wondered whether binding to this region by Upf1

Figure 3. HTS-BABE reveals Upf1 binding to the ribosomal L1 stalk. (**A**) Pymol figure highlighting 14 Upf1 site-specific cysteine variants used for Fe-BABE probing (PDB 2XZL; residues 221–851). Variant Cys sites are shown as purple spheres, and mRNA is shown in blue for reference. A list of the variants used and their domain locations (color-coded to match schematic) is also included. (**B**) MA plot for Upf1 site-specific cysteine variant S335C and its corresponding rRNA cleavage sites identified using HTS-BABE. (**C**) Same as (B) for Upf1 T337C. (**D**) Pymol figure showing positions of S335C (cyan) and T337C (magenta) in relation to 1C domain and the helix 3 residues required for ribosome binding (shown in light purple). (**E**) Primer extension gel to confirm target cleavage sites along L1 stalk for S335C and other variants. (**F**) Same as (E) for an expanded set of Fe-BABE variants. Sample 'S335C-Fe (Fig4B)' was loaded as a positive control.

Figure 4. Upf1 1C domain is essential for L1 stalk binding. (**A**) Schematic of yeast L1 stalk with unique identified cleavage sites from Upf1 variant S335C (cyan) and T337C (magenta). Cleavage sites shared between several variants are noted with black line (25S 2441–2443 and 2462–2464). (**B**) Primer extension gel to confirm target hydroxyl radical cleavage sites along L1 stalk and their dependence on the Upf1 1C domain (for the Upf1 S335C construct). 'o/n' indication means the protein was labeled with Fe-BABE in an overnight reaction on ice, rather than the standard 30 minutes at 30 degrees. (**C**) Pymol model showing the movement of L1 stalk employed to create an 'open configuration.' Open L1 stalk rRNA is shown in blue and L1 protein in green. The 'intermediate-closed' L1 position (PDB 4UG0) is shown in grey for reference as well as the E-site tRNA in pink. (**D**) Pymol model for Upf1 binding to L1 stalk of human 80S ribosomes. (**E**) Close-up view of structural model highlighting Upf1 position in relation to L1 stalk and E-site tRNA, and cleaved residues by Upf1 S335C (cyan) and T337C (magenta). (**F**) Close-up view of Upf1 model and the corresponding cleavage sites mapped to the L1 stalk rRNA.

simply reflects its general RNA binding propensity. Importantly, however, our HTS-BABE analysis with these 14 Upf1 variants did not show significant, reproducible cleavage on other long extended helices on the ribosome such as 18S Helix 16 and expansion segment 6 (Supplementary Figure S4A). And, while we did find modestly enriched cleavage on one long RNA helix (18S U649 in ES6; Supplementary Figure S4B) for several variants, and another variant yielded modestly enriched cleavage on the 18S Helix 16 (Supplementary Figure S3D), there was no evidence for cleavage at these sites using traditional primer extension analysis (Supplementary Figure S4C and D). Taken together, we suggest that these sites are false-positives that emerge from our HTS-BABE experiment. Thus, we argue that the robust and reproducible rRNA cleavage that we observe at the L1 stalk of yeast 80S ribosomes using both HTS-BABE and traditional primer extension analysis is sufficient to define a binding site for Upf1 on the eukaryotic ribosome.

To further validate the Upf1 binding site, we asked whether the L1 stalk cleavages were dependent on the 1C domain of Upf1. We used the Upf1 S335C variant (which yielded a strong signal at bases C2496-U2498 of the L1 stalk along with other weaker cleavage sites in the area) to probe the necessity of the 1C domain by constructing an S335C 1C-12Ala construct (1C domain replaced with twelve alanine residues) and performing the same Fe-BABE probing and primer extension analysis. This experiment revealed a loss of cleavages in the L1 stalk region suggesting that the 1C domain is required for the Upf1 interaction with the ribosome that we define by HTS-BABE (Figure 4B).

Model for Upf1 interaction with ribosomal L1 stalk

With the information provided by our HTS-BABE analysis, we can propose a preliminary model for how Upf1 may interact with the L1 stalk by rigid-body docking of the Upf1 structure on an 80S structure. Importantly, as there is no current structural data for the complete L1 stalk in yeast, we had to model Upf1 onto the structure of the human 80S ribosome where the L1 stalk is more defined (PDB 4UG0) (42). In this human structure, the L1 stalk adopts an 'intermediate-closed' configuration in the presence of a classical-state E-site tRNA, though we anticipate that the human ribosome, like the *E. coli* ribosome, can also adopt an 'open' configuration where L1 swings out away from the ribosome (and the E site is empty). In the 'intermediate-closed' state, we were unable to model a Upf1 molecule bound to the L1 stalk without steric clash in the E site of the ribosome (data not shown), suggesting that ribosomes may have to adopt the open state in order to permit Upf1 binding.

As there are no structures of eukaryotic ribosomes with an open and resolved L1 stalk, we modeled the 'open' state by moving the L1 stalk to align with the open position that has been observed in the *E. coli* 70S ribosome structure; the L1 stalk has been shown to move by as much as 38 Å as it transitions between the 'intermediate-closed' and fully 'open' state (41). As such, we moved the human L1 stalk by approximately 30 Å (Figure 4C) using a previous *E. coli* 70S structure where the L1 stalk is found in an open configura-

tion (PDB 4V9D) (43) as a guide. This open state created enough space between the L1 stalk and ribosomal E site to easily proceed with a rigid-body placement of Upf1.

In this open state, we could model Upf1 bound to the L1 stalk by rigidly positioning the crystal structure for yeast Upf1 (PDB 2XZL; residues 221–851) (15) and using our observed rRNA cleavage sites to guide the positioning (Figure 4D-F). The Upf1 T337C variant strongly cleaved A2484-A2486 of yeast 25S rRNA which corresponds to A4046-A4048 of human 28S rRNA (colored magenta); the S335C variant strongly cleaved C2496–U2498 of yeast 25S rRNA which corresponds to U4058–U4060 human 28S rRNA (colored cyan). This conformation places Upf1 at the edge of the ribosomal E site, with room for the E site tRNA to remain accommodated (Figure 4E), and places the 1C domain where it can make contacts along Helix 76 of the L1 stalk (Figure 4E and F).

In this position, Upf1 is seen to be in close proximity to ribosomal protein eS26 at the mRNA exit channel consistent with previous reports of interaction between the CH domain of Upf1 and eS26 in *S. cerevisiae* (26). While we removed the CH domain from our modeling exercise (as it was not essential for ribosome binding or used in our probing experiments), there is space for the CH domain to be modeled in the conformation observed in the crystal structure (PDB 2XZL) with only minor steric clash with ribosomal protein eS25. As our model relied on movement of the L1 stalk to the open position based on *E. coli* ribosome movements, it is possible that the L1 stalk could move slightly further outward (5–10 Å) to fully accommodate the CH domain. Additionally, as our model includes a mixture of human and yeast components, it is possible that some deviations in ribosome structure near the E site could affect our positioning. Finally, while we propose this model for Upf1:80S interaction, we acknowledge that this positioning depends on just two hydroxyl radical probing constraints (from S335C and T337C Upf1 variants). Future higher resolution approaches (i.e. cryoEM) will be important for increasing the accuracy of our model.

Upf1 does not affect *in vitro* reconstituted elongation, termination, or recycling reactions

Given the binding site of Upf1 on the L1 stalk, and that large-scale movements of this region are known to correlate with the ribosome functional state, we wondered if Upf1 could affect translation directly through interactions with the L1 stalk. To test this possibility, we added purified Upf1 (the Upf1 ΔCH variant used for binding site identification) to several well-established assays in a fully purified yeast *in vitro* reconstituted system (38,44–46). We first added Upf1 to initiated 80S ribosomes and performed an elongation reaction where we monitored penta-peptide (MFFFK) synthesis over time (in the presence of the appropriate aminoacyl-tRNAs and the required yeast elongation factors eEF1A, eEF2 and eEF3). We see no effect of Upf1 on MFFFK synthesis rate (Figure 5A), suggesting that under these conditions, L1 stalk binding by Upf1 has no strong influence on translation elongation. Next we tested Upf1 in an *in vitro* termination reaction, monitoring peptide release by the hydrolytic activity of eRF1. As for the elongation
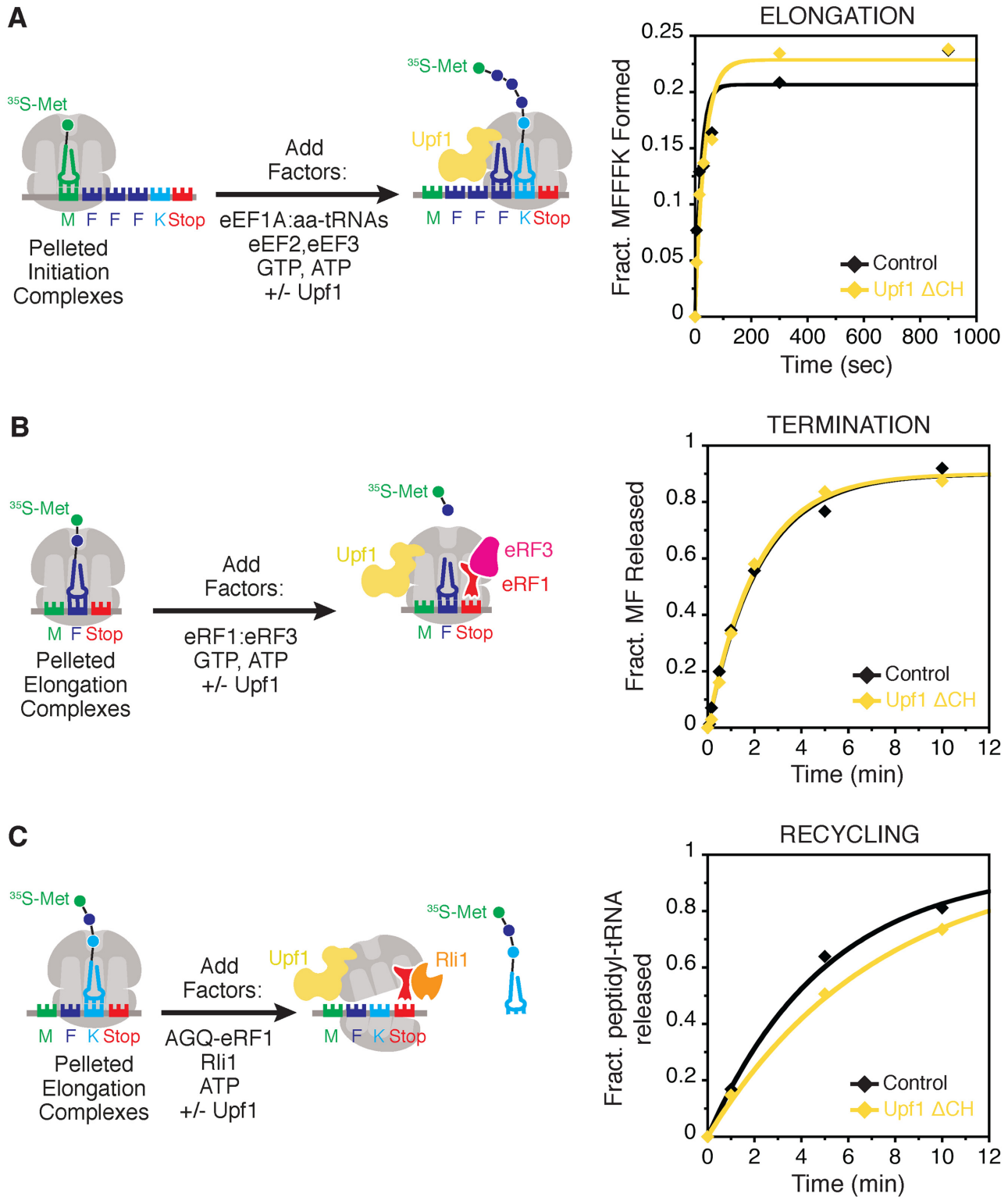
Figure 5. Upf1 does not affect elongation, termination, or recycling in an *in vitro* reconstituted system. (**A**) *In vitro* elongation assay for MFFFK synthesis in the presence and absence of Upf1 ΔCH (residues 221–851). (**B**) *In vitro* termination assay monitoring peptidyl-release by eRF1:eRF3 in the presence and absence of Upf1 ΔCH. (**C**). *In vitro* recycling assay monitoring peptidyl-tRNA release by Rli1 in the presence and absence of Upf1 ΔCH.

reaction, Upf1 addition had no effect on this assay (Figure 5B). Finally, we tested the effect of Upf1 on ribosome subunit recycling catalyzed by Rli1 (ABCE1 in mammals) and eRF1 and, again, observed no effect (Figure 5C). While these assays were repeated multiple times, using multiple different conditions to 'sensitize' the assay, across several preparations of Upf1 including constructs that contained the N-terminal CH domain or were ATPase inactive (data not shown), we were unable to observe any significant biochemical effects. Taken together, these results do not support a direct role for Upf1 in ribosome function, though we recognize that the *in vitro* reconstituted system may lack components important for Upf1 activity to be manifested.

DISCUSSION

The nonsense-mediated decay pathway in eukaryotes which selectively degrades PTC-containing mRNAs depends on three centrally important Upf proteins (Upf1, Upf2, and Upf3). Although much work has been done to shed light on the interactions between the Upfs and other proteins, as well as to characterize the factors involved in mRNA degradation, many questions remain as to how NMD is initiated on the ribosome. Upf1 is the central, catalytic component of the NMD pathway and has been shown to interact with 80S ribosomes, likely in an early step of NMD. However, the molecular details and functional consequence of this interaction remain poorly characterized.

Here, using *in vitro* purified components and a Fe-BABE directed hydroxyl radical approach, we characterize the binding interaction between Upf1 and the 80S ribosome. We show that the Upf1 1C domain, a small alpha-helical insertion in the RecA-like helicase core, is critical for ribosome (Figure 1) and mRNA binding (Supplementary Figure S1C), suggestive of a partitioning event mediated by this domain between the mRNA and ribosome during NMD. To identify the binding site for Upf1 on the 80S ribosome, we developed a high throughput sequencing-based Fe-BABE directed hydroxyl radical probing method (HTS-BABE) (Figure 2), and identified the L1 stalk of the 25S rRNA as the binding site of Upf1 (Figure 3). We subsequently verified this interaction to be dependent on the 1C domain of Upf1 and assembled a model of Upf1 binding to the L1 stalk on human 80S ribosomes (Figure 4).

Despite the robust nature of the interaction that we define, the molecular details of the Upf1:80S interaction were somewhat surprising to us. The NMD pathway must depend on recognition of a premature termination codon, an event that occurs in the ribosomal A site, while our data suggest that Upf1 binds on the other side of the ribosome in the region proximal to the E site. While other published data have suggested that Upf1 binding occurs in this region near eS26 (26), it remains unclear how this binding site is connected to proper initiation of NMD. We speculate that Upf1 binding to the L1 stalk could have long-range effects on the ribosome that impact A site reactivity as observed for a number of other translation factors (eEF3, eIF5A, EFP, and EttA) (38–40,47–53). This is especially possible given the highly dynamic nature of the L1 stalk as it moves from a 'closed' position with hybrid-state tRNAs after peptidyl-transfer, to an 'open' conformation with a vacant E site.

As translation termination and recycling both occur at termination codons (a hallmark of NMD) and the ribosome would be anticipated to be in a classical state during these events (54–57), it is possible that Upf1 could impact one of these functions through long-range allosteric effects (58). Additionally, while our attempts at observing a direct effect for Upf1 in translation elongation, termination, or recycling using an established *in vitro* reconstituted system were unsuccessful (Figure 5), it is possible that our reactions lack some key component. Whatever the mechanism of action for Upf1 might be, our identification of the 1C domain as critical for the Upf1:80S interaction is strongly supported by previous work indicating that this domain is essential for NMD (28).

Finally, we hope that our HTS-BABE approach will enhance structural determination by hydroxyl radical probing methods, or be used in conjunction with other methods such as x-ray crystallography and cryoEM. While the resolution of this method is not atomic, it could be used to cross validate cryoEM data when the identity of certain volumes is unknown, help orient a molecule if sufficient resolution cannot be obtained, or be used when molecules are flexible or otherwise suboptimal for structural determination. In the case of Upf1, the eukaryotic ribosomal L1 stalk remains poorly characterized by these other structural methods, likely because of its inherent flexibility, and may be challenging to solve unless it can be trapped in a stable conformation. Future pursuits to stabilize and determine the complete Upf1:80S structure will be required to support our understanding of how Upf1 might initiate NMD at a terminating ribosome.

AVAILABILITY

Sequencing data and mapped read counts have been deposited in GEO with accession number GSE104072. HTS-BABE analysis scripts can be found at: https://github.com/greenlabjhmi/HTS-BABE.

SUPPLEMENTARY DATA

Supplementary Data are available at NAR online.

ACKNOWLEDGEMENTS

FUNDING

Conflict of interest statement. None declared.

REFERENCES

1. Shoemaker,C.J. and Green,R. (2012) Translation drives mRNA quality control. *Nat. Struct. Mol. Biol.*, **19**, 594–601.
2. Holbrook,J.A., Neu-Yilik,G., Hentze,M.W. and Kulozik,A.E. (2004) Nonsense-mediated decay approaches the clinic. *Nat. Genet.*, **36**, 801–808.
3. He,F., Peltz,S.W., Donahue,J.L., Rosbash,M. and Jacobson,A. (1993) Stabilization and ribosome association of unspliced pre-mRNAs in a yeast upf1- mutant. *Proc. Natl. Acad. Sci. U.S.A.*, **90**, 7034–7038.
4. Mitrovich,Q.M. and Anderson,P. (2000) Unproductively spliced ribosomal protein mRNAs are natural targets of mRNA surveillance in C. elegans. *Genes Dev.*, **14**, 2173–2184.
5. Mendell,J.T., Sharifi,N.A., Meyers,J.L., Martinez-Murillo,F. and Dietz,H.C. (2004) Nonsense surveillance regulates expression of diverse classes of mammalian transcripts and mutes genomic noise. *Nat. Genet.*, **36**, 1073–1078.
6. Welch,E.M. and Jacobson,A. (1999) An internal open reading frame triggers nonsense-mediated decay of the yeast SPT10 mRNA. *EMBO J.*, **18**, 6134–6145.
7. Marquardt,S., Hazelbaker,D.Z. and Buratowski,S. (2011) Distinct RNA degradation pathways and 3' extensions of yeast non-coding RNA species. *Transcription*, **2**, 145–154.
8. Smith,J.E., Alvarez-Dominguez,J.R., Kline,N., Huynh,N.J., Geisler,S., Hu,W., Coller,J. and Baker,K.E. (2014) Translation of small open reading frames within unannotated RNA transcripts in Saccharomyces cerevisiae. *Cell Rep.*, **7**, 1858–1866.
9. Kervestin,S. and Jacobson,A. (2012) NMD: a multifaceted response to premature translational termination. *Nat. Rev. Mol. Cell Biol.*, **13**, 700–712.
10. Lelivelt,M.J. and Culbertson,M.R. (1999) Yeast Upf proteins required for RNA surveillance affect global expression of the yeast transcriptome. *Mol. Cell. Biol.*, **19**, 6710–6719.
11. Medghalchi,S.M., Frischmeyer,P.A., Mendell,J.T., Kelly,A.G., Lawler,A.M. and Dietz,H.C. (2001) Rent1, a trans-effector of nonsense-mediated mRNA decay, is essential for mammalian embryonic viability. *Hum. Mol. Genet.*, **10**, 99–105.
12. Rehwinkel,J., Letunic,I., Raes,J., Bork,P. and Izaurralde,E. (2005) Nonsense-mediated mRNA decay factors act in concert to regulate common mRNA targets. *RNA*, **11**, 1530–1544.
13. Culbertson,M.R., Underbrink,K.M. and Fink,G.R. (1980) Frameshift suppression Saccharomyces cerevisiae. II. Genetic properties of group II suppressors. *Genetics*, **95**, 833–853.
14. Leeds,P., Wood,J.M., Lee,B.S. and Culbertson,M.R. (1992) Gene products that promote mRNA turnover in Saccharomyces cerevisiae. *Mol. Cell. Biol.*, **12**, 2165–2177.
15. Chakrabarti,S., Jayachandran,U., Bonneau,F., Fiorini,F., Basquin,C., Domcke,S., Le Hir,H. and Conti,E. (2011) Molecular mechanisms for the RNA-dependent ATPase activity of Upf1 and its regulation by Upf2. *Mol. Cell*, **41**, 693–703.
16. Chamieh,H., Ballut,L., Bonneau,F. and Le Hir,H. (2008) NMD factors UPF2 and UPF3 bridge UPF1 to the exon junction complex and stimulate its RNA helicase activity. *Nat. Struct. Mol. Biol.*, **15**, 85–93.
17. Czaplinski,K., Weng,Y., Hagan,K.W. and Peltz,S.W. (1995) Purification and characterization of the Upf1 protein: a factor involved in translation and mRNA degradation. *RNA*, **1**, 610–623.
18. Weng,Y., Czaplinski,K. and Peltz,S.W. (1998) ATP is a cofactor of the Upf1 protein that modulates its translation termination and RNA binding activities. *RNA*, **4**, 205–214.
19. Schoenberg,D.R. and Maquat,L.E. (2012) Regulation of cytoplasmic mRNA decay. *Nat. Rev. Genet.*, **13**, 246–259.
20. Maquat,L.E. (2004) Nonsense-mediated mRNA decay: splicing, translation and mRNP dynamics. *Nat. Rev. Mol. Cell Biol.*, **5**, 89–99.
21. Le Hir,H., Gatfield,D., Izaurralde,E. and Moore,M.J. (2001) The exon-exon junction complex provides a binding platform for factors involved in mRNA export and nonsense-mediated mRNA decay. *EMBO J.*, **20**, 4987–4997.
22. Metze,S., Herzog,V.A., Ruepp,M.D. and Muhlemann,O. (2013) Comparison of EJC-enhanced and EJC-independent NMD in human cells reveals two partially redundant degradation pathways. *RNA*, **19**, 1432–1448.
23. Losson,R. and Lacroute,F. (1979) Interference of nonsense mutations with eukaryotic messenger RNA stability. *Proc. Natl. Acad. Sci. U.S.A.*, **76**, 5134–5137.
24. Takeshita,K., Forget,B.G., Scarpa,A. and Benz,E.J Jr (1984) Intranuclear defect in beta-globin mRNA accumulation due to a premature translation termination codon. *Blood*, **64**, 13–22.
25. Atkin,A.L., Altamura,N., Leeds,P. and Culbertson,M.R. (1995) The majority of yeast UPF1 co-localizes with polyribosomes in the cytoplasm. *Mol. Biol. Cell*, **6**, 611–625.
26. Min,E.E., Roy,B., Amrani,N., He,F. and Jacobson,A. (2013) Yeast Upf1 CH domain interacts with Rps26 of the 40S ribosomal subunit. *RNA*, **19**, 1105–1115.
27. Czaplinski,K., Ruiz-Echevarria,M.J., Paushkin,S.V., Han,X., Weng,Y., Perlick,H.A., Dietz,H.C., Ter-Avanesyan,M.D. and Peltz,S.W. (1998) The surveillance complex interacts with the translation release factors to enhance termination and degrade aberrant mRNAs. *Genes Dev.*, **12**, 1665–1677.
28. Cheng,Z., Muhlrad,D., Lim,M.K., Parker,R. and Song,H. (2007) Structural and functional insights into the human Upf1 helicase core. *EMBO J.*, **26**, 253–264.
29. Powers,T. and Noller,H.F. (1995) Hydroxyl radical footprinting of ribosomal proteins on 16S rRNA. *RNA*, **1**, 194–209.
30. Dixon,W.J., Hayes,J.J., Levin,J.R., Weidner,M.F., Dombroski,B.A. and Tullius,T.D. (1991) Hydroxyl radical footprinting. *Methods Enzymol.*, **208**, 380–413.
31. Rana,T.M. and Meares,C.F. (1991) Transfer of oxygen from an artificial protease to peptide carbon during proteolysis. *Proc. Natl. Acad. Sci. U.S.A.*, **88**, 10578–10582.
32. Joseph,S., Weiser,B. and Noller,H.F. (1997) Mapping the inside of the ribosome with an RNA helical ruler. *Science*, **278**, 1093–1098.
33. Heilek,G.M. and Noller,H.F. (1996) Site-directed hydroxyl radical probing of the rRNA neighborhood of ribosomal protein S5. *Science*, **272**, 1659–1662.
34. Wilson,K.S. and Noller,H.F. (1998) Mapping the position of translational elongation factor EF-G in the ribosome by directed hydroxyl radical probing. *Cell*, **92**, 131–139.
35. Culver,G.M., Cate,J.H., Yusupova,G.Z., Yusupov,M.M. and Noller,H.F. (1999) Identification of an RNA-protein bridge spanning the ribosomal subunit interface. *Science*, **285**, 2133–2136.
36. He,S.L. and Green,R. (2010) Visualization of codon-dependent conformational rearrangements during translation termination. *Nat. Struct. Mol. Biol.*, **17**, 465–470.
37. Kielpinski,L.J. and Vinther,J. (2014) Massive parallel-sequencing-based hydroxyl radical probing of RNA accessibility. *Nucleic Acids Res.*, **42**, e70.
38. Schuller,A.P., Wu,C.C., Dever,T.E., Buskirk,A.R. and Green,R. (2017) eIF5A Functions Globally in Translation Elongation and Termination. *Mol. Cell*, **66**, 194–205.
39. Gutierrez,E., Shin,B.S., Woolstenhulme,C.J., Kim,J.R., Saini,P., Buskirk,A.R. and Dever,T.E. (2013) eIF5A promotes translation of polyproline motifs. *Mol. Cell*, **51**, 35–45.
40. Schmidt,C., Becker,T., Heuer,A., Braunger,K., Shanmuganathan,V., Pech,M., Berninghausen,O., Wilson,D.N. and Beckmann,R. (2016) Structure of the hypusinylated eukaryotic translation factor eIF-5A bound to the ribosome. *Nucleic Acids Res.*, **44**, 1944–1951.
41. Mohan,S. and Noller,H.F. (2017) Recurring RNA structural motifs underlie the mechanics of L1 stalk movement. *Nat. Commun.*, **8**, 14285.
42. Khatter,H., Myasnikov,A.G., Natchiar,S.K. and Klaholz,B.P. (2015) Structure of the human 80S ribosome. *Nature*, **520**, 640–645.
43. Dunkle,J.A., Wang,L., Feldman,M.B., Pulk,A., Chen,V.B., Kapral,G.J., Noeske,J., Richardson,J.S., Blanchard,S.C. and Cate,J.H. (2011) Structures of the bacterial ribosome in classical and hybrid states of tRNA binding. *Science*, **332**, 981–984.
44. Shoemaker,C.J. and Green,R. (2011) Kinetic analysis reveals the ordered coupling of translation termination and ribosome recycling in yeast. *Proc. Natl. Acad. Sci. U.S.A.*, **108**, E1392–E1398.
45. Eyler,D.E. and Green,R. (2011) Distinct response of yeast ribosomes to a miscoding event during translation. *RNA*, **17**, 925–932.

46. Shoemaker,C.J., Eyler,D.E. and Green,R. (2010) Dom34:Hbs1 promotes subunit dissociation and peptidyl-tRNA drop-off to initiate no-go decay. *Science*, **330**, 369–372.

47. Blaha,G., Stanley,R.E. and Steitz,T.A. (2009) Formation of the first peptide bond: the structure of EF-P bound to the 70S ribosome. *Science*, **325**, 966–970.

48. Andersen,C.B., Becker,T., Blau,M., Anand,M., Halic,M., Balar,B., Mielke,T., Boesen,T., Pedersen,J.S., Spahn,C.M. *et al.* (2006) Structure of eEF3 and the mechanism of transfer RNA release from the E-site. *Nature*, **443**, 663–668.

49. Chen,B., Boel,G., Hashem,Y., Ning,W., Fei,J., Wang,C., Gonzalez,R.L. Jr, Hunt,J.F. and Frank,J. (2014) EttA regulates translation by binding the ribosomal E site and restricting ribosome-tRNA dynamics. *Nat. Struct. Mol. Biol.*, **21**, 152–159.

50. Boel,G., Smith,P.C., Ning,W., Englander,M.T., Chen,B., Hashem,Y., Testa,A.J., Fischer,J.J., Wieden,H.J., Frank,J. *et al.* (2014) The ABC-F protein EttA gates ribosome entry into the translation elongation cycle. *Nat. Struct. Mol. Biol.*, **21**, 143–151.

51. Doerfel,L.K., Wohlgemuth,I., Kothe,C., Peske,F., Urlaub,H. and Rodnina,M.V. (2013) EF-P is essential for rapid synthesis of proteins containing consecutive proline residues. *Science*, **339**, 85–88.

52. Triana-Alonso,F.J., Chakraburtty,K. and Nierhaus,K.H. (1995) The elongation factor 3 unique in higher fungi and essential for protein biosynthesis is an E site factor. *J. Biol. Chem.*, **270**, 20473–20478.

53. Ude,S., Lassak,J., Starosta,A.L., Kraxenberger,T., Wilson,D.N. and Jung,K. (2013) Translation elongation factor EF-P alleviates ribosome stalling at polyproline stretches. *Science*, **339**, 82–85.

54. Brown,A., Shao,S., Murray,J., Hegde,R.S. and Ramakrishnan,V. (2015) Structural basis for stop codon recognition in eukaryotes. *Nature*, **524**, 493–496.

55. Matheisl,S., Berninghausen,O., Becker,T. and Beckmann,R. (2015) Structure of a human translation termination complex. *Nucleic Acids Res.*, **43**, 8615–8626.

56. Preis,A., Heuer,A., Barrio-Garcia,C., Hauser,A., Eyler,D.E., Berninghausen,O., Green,R., Becker,T. and Beckmann,R. (2014) Cryoelectron microscopic structures of eukaryotic translation termination complexes containing eRF1-eRF3 or eRF1-ABCE1. *Cell Rep.*, **8**, 59–65.

57. Shao,S., Murray,J., Brown,A., Taunton,J., Ramakrishnan,V. and Hegde,R.S. (2016) Decoding mammalian ribosome-mRNA states by translational GTPase complexes. *Cell*, **167**, 1229–1240.

58. Nierhaus,K.H. (1990) The allosteric three-site model for the ribosomal elongation cycle: features and future. *Biochemistry*, **29**, 4997–5008.

59. Youngman,E.M., Brunelle,J.L., Kochaniak,A.B. and Green,R. (2004) The active site of the ribosome is composed of two layers of conserved nucleotides with distinct roles in peptide bond formation and peptide release. *Cell*, **117**, 589–599.

60. Jiang,H., Lei,R., Ding,S.W. and Zhu,S. (2014) Skewer: a fast and accurate adapter trimmer for next-generation sequencing paired-end reads. *BMC Bioinformatics*, **15**, 182.

61. Dobin,A., Davis,C.A., Schlesinger,F., Drenkow,J., Zaleski,C., Jha,S., Batut,P., Chaisson,M. and Gingeras,T.R. (2013) STAR: ultrafast universal RNA-seq aligner. *Bioinformatics*, **29**, 15–21.